HHS Public Access

Author manuscript

Adv Mater Technol. Author manuscript; available in PMC 2019 December 04.

Published in final edited form as:

Adv Mater Technol. 2018 December ; 3(12): . doi:10.1002/admt.201800233.

Stereolithography for Personalized Left Atrial Appendage Occluders

Sanlin S. Robinson,
Department of Materials Science and Engineering, Cornell University, Ithaca, NY 14853, USA

Dalio Institute of Cardiovascular Imaging, Department of Radiology, New York-Presbyterian, Hospital and Weill Cornell Medicine, New York, NY 10021, USA

Cameron A. Aubin,
Sibley School of Mechanical and Aerospace Engineering, Cornell University, Ithaca, NY 14853, USA

Thomas J. Wallin,
Department of Materials Science and Engineering, Cornell University, Ithaca, NY 14853, USA

Saleh Gharaie,
Dalio Institute of Cardiovascular Imaging, Department of Radiology, New York-Presbyterian, Hospital and Weill Cornell Medicine, New York, NY 10021, USA

Patricia A. Xu,
Sibley School of Mechanical and Aerospace Engineering, Cornell University, Ithaca, NY 14853, USA

Kaiyang Wang,
Department of Materials Science and Engineering, Cornell University, Ithaca, NY 14853, USA

Simon N. Dunham,
Dalio Institute of Cardiovascular Imaging, Department of Radiology, New York-Presbyterian, Hospital and Weill Cornell Medicine, New York, NY 10021, USA

Bobak Mosadegh,
Dalio Institute of Cardiovascular Imaging, Department of Radiology, New York-Presbyterian, Hospital and Weill Cornell Medicine, New York, NY 10021, USA

Robert F. Shepherd
Department of Materials Science and Engineering, Cornell University, Ithaca, NY 14853, USA

Sibley School of Mechanical and Aerospace Engineering, Cornell University, Ithaca, NY 14853, USA

Abstract

rfs247@cornell.edu.

Conflict of Interest
The authors declare no conflict of interest.

Supporting Information
Supporting Information is available from the Wiley Online Library or from the author.

Advancements in 3D additive manufacturing have spurred the development of effective patient-specific medical devices. Prior applications are limited to hard materials, however, with few implementations of soft devices that better match the properties of natural tissue. This paper introduces a rapid, low cost, and scalable process for fabricating soft, personalized medical implants via stereolithography of elastomeric polyurethane resin. The effectiveness of this approach is demonstrated by designing and manufacturing patient-specific endocardial implants. These devices occlude the left atrial appendage, a complex structure within the heart prone to blood clot formation in patients with atrial fibrillation. Existing occluders permit residual blood flow and can damage neighboring tissues. Here, the robust mechanical properties of the hollow, printed geometries are characterized and stable device anchoring through in vitro benchtop testing is confirmed. The soft, patient-specific devices outperform non-patient-specific devices in embolism and occlusion experiments, as well as in computational fluid dynamics simulations.

Keywords

3D printing; elastomers; medical devices; patient-specific; stereolithography

Mass-produced medical implants typically come in several standard geometries and sizes that often fail to address the various patient morphologies encountered, particularly when a patient's anatomy is in a diseased state. With advancements in high-resolution imaging, segmentation software, and rapid prototyping,[1–4] the development of patient-specific implants has become more accessible to the medical community. To date, personalized implants have been fabricated for a variety of medical needs such as airway disorders,[5] mitral valve insufficiencies,[6,7] craniomaxillofacial defects,[8,9] and orthopedic replacements.[10–12] Due to manufacturing and chemistry limitations, most of these custom implants require fabrication from high elastic modulus ($E > 1$ GPa) materials that are mechanically dissimilar to the soft tissues of the human body ($E < 1$ MPa).[13] Such rigid devices fail to conform to neighboring anatomical structures, concentrate stress, and can perforate tissues.[14] Here, we present stereolithography (SLA) of elastomeric polyurethane (EPU) as a fast (≈3 cm h^{-1} draw-rate), low-cost ($0.25 mL^{-1} of material), and scalable 3D printing process for fabricating patient-specific (P-S) medical implants. As a demonstration, we have fabricated patient-specific left atrial appendage (LAA) occluders (Figure 1a) for those at high risk of blood clot formation due to atrial fibrillation (AF). In our previous publication,[15] we fabricated these LAA occluders using replica molding of silicones; here, we demonstrate a 40% reduction in wall thickness, a twofold increase in burst pressures, and an improved anatomic matching to the appendages' structure due to the higher resolution of SLA printing.

Patients with AF have nearly a five times greater risk of stroke due to cardiac emboli,[16] with greater than 50% of these emboli originating in the LAA, possibly due to the low flow velocities of blood within the complex structure.[17] Blood thinners are currently the first line of therapy to prevent stroke in high-risk patients. These drugs, however, are only effective in a narrow therapeutic window, require frequent and ongoing monitoring, increase the risk of internal bleeding, and can negatively interact with the individual's physiology or other drugs.[18] Therefore, surgical removal or mechanical occlusion of the LAA is the

recommended alternative for stroke prophylaxis.[19–21] Unfortunately, conventional surgical resection of the appendage not only hinders the contractile function of the remaining left atrial tissue[22] but also can result in incomplete closure (≈36% of cases) and commensurate risk of stroke.[23,24] These risks lead many practitioners to avoid recommending surgical interventions that remove or remodel the LAA. As an alternative, mechanical LAA occlusion devices that employ a self-expanding metal alloy (nitinol) cage are now available in a set number of sizes. These occluders deploy into a round dome that caps the ostium of the appendage.[19–21] Implantation of these rigid devices requires physically anchoring them using hooks, which concentrate mechanical stress and can cause tears in the thin-walled tissue of the LAA. Additionally, due to the high variability of LAA morphologies, standardized, off-the-shelf occluder geometries often fail to completely block an ostium from residual blood flow.[14,15,25,26]

Recently, our labs demonstrated the efficacy of patient-specific, soft, hollow LAA occluders[15] implanted in a canine model to address the issues of incomplete occlusion, perforation of LAA tissue, and device anchoring. Construction with elastomers is key to this advancement—the highly compliant endovascular devices are selectively inflated to fully conform to the complex LAA morphology at low volumes, which minimizes stress and damage to the surrounding tissues. Though fabricated via rapid prototyping (i.e., replica molding, lamination, and dipcoating), the workflow for constructing personalized occluders remains laborious and time-consuming; we required at least 3 d to fabricate the patient-specific designs. Additionally, this manufacturing strategy is incompatible with potentially unmoldable morphologies and requires a lamination step that introduces a seam, which leads to nonuniform wall thicknesses and reduces mechanical integrity due to these regions of high stress concentrations. Herein, we demonstrate a rapid approach where we perform segmentation of the LAA from computed tomography (CT) scans, create a computer-aided design (CAD), and 3D print the custom geometry to realize a monolithic, thin-walled elastomeric LAA occluder (Figure 1). This process requires only ≈12 h.

Though various 3D printing technologies (e.g., direct ink writing, fused deposition modeling, selective laser sintering)[7,27–29] have been used in medicine, we chose to use SLA. Based on layer-by-layer solidification of a liquid resin in response to photopatterned light (Figure S1, Supporting Information), SLA enables direct fabrication of complex, hollow elastomeric architectures with feature sizes on the order of 100 μm[2,30,31] Additionally, by projecting multiple images onto the same build stage, we can rapidly (t_{print} ≈ 1.5 h) manufacture in a single print (i) multiple design variations for the same patient (i.e., iterate design complexity; Figure S2a, Supporting Information), (ii) multiple occluders for different patients (Figures S2b and S3, Supporting Information), and (iii) multiple copies of one design for one patient (i.e., scale-up manufacturing; Figure 1c).

We employed noninvasive, human cardiac CT scans to guide the design of patient-specific occluders, a method thoroughly described previously by Robinson et al. (Figure 1b).[15] Briefly, we used an open-source software (ITK-Snap, University of Pennsylvania) to perform semiautomatic image segmentation on the left heart blood volume from human CT scans. Next, an additional image processing software (Geomagic Wrap, 3D Systems) isolated the LAA, smoothed the surface, and shelled the object for 3D printing as a hollow

structure with a wall thickness of 300 μm. To prepare the design for direct printing, we used SolidWorks (Dassault Systems) to (i) add a valve to the ostial surface of the occluder, and (ii) insert drainage holes to reduce vacuum forces that occur during SLA printing of hollow structures (Figure 1b).

We used a high-resolution (75 μm pixel), projection-based SLA printer (M1, Carbon, Inc.) and a commercial elastomeric polyurethane (EPU, Carbon) resin to directly print custom LAA occluder designs (Figure 1c). With a 141 mm × 79 mm build stage, 10–15 occluders can be printed at once, greatly increasing the fabrication speed over previous methods. After printing, the base material is not fully polymerized, and the resulting *green bodies* are fragile and covered in liquid resin (Figure 1c). We used isopropyl alcohol to gently clean resin off both the external and internal surfaces. The drainage holes that allowed for venting of the hollow prints, also aid in the removal of encapsulated, unreacted resin inside the occluders. Applying a thin layer of fresh resin over these holes, followed by exposure ($t \approx 10$ s) under a UV light source (ECE 5000, Dymax Inc.) sealed the green body. A postprocessing thermal treatment (120 °C for 8 h) fully cured the EPU material to obtain the full elastomeric and mechanical properties (Figures 1c and 2a). Finally, we injected silicone prepolymer (Ecoflex 00–30, Smooth-On) into the cavity of the valve where it interlocks and cures with printed crossbars to create a self-sealing valve (Figure 2a). By iterating this process with a representative geometry (e.g., Chicken Wing) obtained from a CT scan, we empirically determined the minimum wall thickness ($t = 318.6 \pm 49$ μm) compatible with our printing process (Figure 2b). Replica molding pathways for similar elastomeric occlusion devices could only achieve thickness with large dimensional variance, $t = 500 \pm 125$ μm.[15] The final printed occluder, when compressed, fits into an 18 Fr catheter ($d = 6$ mm) for surgical intervention (Figure 2c).

Our material choice also imparts important mechanical performance to the printed devices. Compared to other available SLA materials, EPU is an excellent candidate owing to its large ultimate strains ($\gamma_{ult} > 300\%$; Figure 2a) and high tear strength ($\Gamma_{tear} = 23 \pm 3$ kN m^{-1}). Combined, these properties lead to a robust, highly deformable device even when dimensions are miniaturized. Despite having a 40% thinner wall, these occluders operate safely at pressures and volumes ($\Delta P > 60$ kPa, $\Delta V > 50$ mL; Figure 2c and Figure S4, Supporting Information) that exceed the corresponding failure regimes of their replica molded silicone counterparts ($\Delta P_{burst} \approx 30$ kPa, $\Delta V_{burst} \approx 40$ mL).[15]

One of the primary challenges in using SLA for biomedical applications is the entrapment of potentially cytotoxic photoinitiator and unreacted monomer species inside printed parts.[32] Additional solvent soaking, ultraviolet light exposure, and thermal baking can aid in extracting these unwanted compounds from printed devices before their use in biological applications.[33,34] Diphenyl(2,4,6-trimethylbenzoyl)phosphine oxide (TPO) is the primary photoinitiator compound in the EPU resin, though its exact concentration is proprietary information. We used Fourier-transform infrared spectroscopy (FTIR) to detect the presence of unreacted TPO photoinitiator in our printed EPU parts (Figure S5, Supporting Information). For this experiment, we printed EPU cubes ($V = 1$ cm^3) and subjected them to different levels of postprocessing. The printed samples were swelled in tetrahydrofuran (THF) for 48 h to extract any unreacted compounds, before performing FTIR measurements

on the solvent samples. We were unable to detect the photoinitiator compound when comparing the spectra of the solvent samples to a control containing TPO in THF. We believe that the additional postprocessing steps, such as UV curing the parts after printing, which has been shown to reduce cytotoxicity of SLA prints,[34] as well as baking the parts for 8 h at high temperatures contribute to a more fully polymerized structure, though it is probable that some small concentration of unreacted compounds persists within the parts.

Another concern with implanted occluders is the possibility of device embolization into the left atrium. To probe the long-term viability of our printed geometries, we conducted in vitro pull-out tests at different device inflation volumes, $V_{\text{inflation}} = (V_{\text{injected}}/V_{\text{rest}}) \times 100\%$ (figure 3a). We 3D printed a custom attachment for the bottom grip of our tensile tester (Zwick & Roell, z010) that replicates the Chicken Wing LAA anatomy (Figure 3b, and Figure S6, Supporting Information). We implanted either a patient-specific or spherical occluder ($r_{\text{rest}} = 8.75$ mm) into this synthetic LAA. After implantation, we applied an increasing tensile force to the ostial surface of the occluder until it ejected from the simulated appendage (Figure 3b, and Figure S6, Supporting Information). We report the maximum force during separation as a function of inflation volume (Figure 3a, Table 1). For the P-S morphology, we estimated a minimum occlusion volume of $V_{\text{inflation}} \approx 200\%$ (Figure S7, Supporting Information). This volume corresponds to a pull-out force of $F_{\text{pull-out}} \approx 14.9 \pm 1.47$ N, which suggests that our designs will anchor firmly within the LAA. Increasing the volume of both the P-S and spherical occluders logically increases the pullout forces, but likely impinges upon the adjacent anatomy. In particular, the spherical samples with large inflation volumes ($V_{\text{inflation}} > 150\%$) visibly deformed the simulated LAA, which is consistent with our observations that non-P-S geometries have the potential to strain and damage both the LAA and neighboring tissues while attempting to fully occlude the ostium.

Whereas the pull-out measurements were made on a static appendage, the in vivo atrial environment is dynamic. The oscillating pressures within the heart, coupled with the expansion and contraction of the atria may contribute to device embolism at forces less than the above measured thresholds. Here, we simulated the LAA anatomy using a silicone (Ecoflex 00–30, Smooth-on) phantom attached to an idealized left atrium flow loop (Figure 3c, and Figure S8, Supporting Information). After implanting our printed device, we controlled the operation of two pumps at pulsatile flow ($f \approx 1$ Hz) and pressure regimes ($\Delta P \approx 15$ kPa) that approximated the systolic and diastolic behavior of the left heart ($\Delta P \approx 16$ kPa; Figure 3c).[35] Table 1 notes any embolism event or damage to the LAA phantom during subsequent continuous operation for 48 h. We found that both P-S and spherical occluders embolized when they were underinflated, $V_{\text{inflation}} \approx 50\%$ (Figure S9, Supporting Information). We also observed that overinflation ($V_{\text{inflation}} > 200\%$) of spherical occluders tore the silicone LAA within the first 24 h (Figure S10, Supporting Information).

Currently available mechanical closure devices are round in shape, while the ostium of most LAAs are elliptical. This mismatch in geometry causes large crevices to form on either side of implanted occluders; these cavities can lead to residual flow of blood into the LAA and to clots forming on or around the device. To ensure stable anchoring and to mitigate residual flow, these round devices are typically oversized by 8–20%[36] While this practice helps eliminate blood flowing into the appendage, it does not diminish—and may worsen—the

severity of the crevices between the occluder and the atrial wall. The ability of our printed LAA to change volume in a “balloon-like” manner is a key differentiator compared to existing LAA occluders, and allows them to conform to the LAA anatomy. These occluders can be backfilled with a variety of materials depending on the preference of the interventionalist; depending on their comfort with the procedure they may chose materials that cure more quickly or more slowly to ensure enough time for proper orientation. The atrial-facing geometry of our occluders was designed from the CT scans to exactly match the existing anatomy.

We used computational fluid dynamics (CFD) to analyze the atrial-facing geometry of patient-specific and spherical occluders (Figure 4). We used SolidWorks to assemble either a P-S or spherical occluder into the appendage of a Chicken Wing LAA morphology. After creating a solid body and mesh we then performed the flow analysis. We overlaid the contour results from the wall shear stress of both the P-S and spherical geometries over their left heart models (Figure 4b,c). Our observations indicate that the regions along the edges of the spherical occluder had very low wall shear stress regimes (Figure 4c), which prior studies have correlated with clot formation.[37] These areas of low wall shear stress were not as pronounced in the P-S design (Figure 4b), likely due to better conformal matching of the internal atrial wall.

Although medical 3D printing is most commonly used for education and surgical planning,[29,38–40] we have demonstrated the fabrication of patient-specific medical devices as another promising application. We developed a strategy for rapidly producing a left atrial appendage occluder designed specifically for an individual patient suffering from atrial fibrillation. These occluders are printed using elastomeric polyurethane and function balloons that can conform to a patient’s anatomy once inflated. While previous manufacturing strategies are too laborious for practical implementation[15] our 3D printing technique allows for fabrication of 10–15 patient-specific occluders in under 12 h for less than $0.50 per device. These hollow occluders possess thin walls ($t \approx 318.6 \pm 49$ gm) that enable surgical implantation, as well as robust mechanical properties ($\Delta P_{burst} > 60$ kPa, $\Delta V_{burst} > 50$ mL). Furthermore, SLA printing allows us to create different objects and devices with complex geometries that cannot be produced using other mold-based fabrication techniques (Figure S11, Supporting Information). We believe our method can be more broadly applied to other areas of medicine, where soft materials and patient-specificity are needed (e.g., stents, valves, and prosthetics).

In brief, using CT segmentation[15] we obtained patient-specific volumetric renderings that are compatible with SLA printing using elastomeric material. Post printing, we added a self-sealing silicone valve to enable rapid inflation and deflation of these thin-walled elastomeric balloons. We demonstrated the stable anchoring of these occluders within a simulated appendage by measuring the pull-out force, and tested the long-term implantation of the occluder. We found that the pull-out force needed to dislodge a fully inflated P-S occluder was $F_{pull\text{-}out} \approx 14.9 \pm 1.47$ N, and that only underinflated occluders ($V_{inflation} \approx 50\%$) were not stable over long periods of time in our benchtop flow loop. Using CFD, we concluded that spherical occluder geometries have much lower shear regions which would likely cause more clots. These low shear regions were not observed in the P-S device. Though we did not

investigate hemocompatibility of our base EPU material, prior work demonstrates a straightforward process to sterilize and coat a hemocompatible material on to the surface of the device.[15] Future research should include long-term in vivo studies in order to assess biocompatibility, hemocompatibility, endothelialization of the device at blood contacting surfaces, and long-term stability of the device after implantation.

Experimental Section

Uniaxial Tensile Tests

Tensile tests were performed according to ISO 37 on a Zwick Roell z010 instrument. All tests were conducted at room temperatures using a 10 kN load cell and a strain rate of 200 mm min^{-1}. The data were averaged across common strain range and plotted with standard deviation ($n = 11$). Every 35 points were skipped to make data more visible.

Thickness Variation

Three specimens were sampled from three different occluders, for a total of nine samples. A razor blade was used to slice portions of the printed occluder in a variety of areas. An optical microscope (Zeiss) was then used to image these samples against a reticle of known dimensions (Figure 2b, right). This reticle was fabricated by etching lines with set dimensions into acrylic using a laser cutter (Epilog Zing 50W, Epilog Laser). The images were processed using ImageJ by measuring each specimen in three positions. The mean and standard deviation were calculated using Microsoft Excel (Excel for Mac, Version 15.32, 2017).

Pressure-Volume Tests

All pressure-volume data in this paper were collected using custom LabVIEW code (Code can be made available upon request, National Instruments). The code controlled the input volume through a programmable syringe pump (NE-1000, New Era Pump Systems Inc.) and recorded the output pressure data from a pressure transducer (0–100 PSI, TDH30-CG-0100–03-D004, Transducers direct). These tests were performed on 14 occluders (7 patient-specific, 7 spherical geometries). Each sample was inflated and deflated five times. To remove the initial inelastic effects in the stress-strain behavior of the base polymer, only the fifth recording was used to determine the mean and standard deviation between the samples (Figure 2c).

Pull-Out Tests

To characterize the pull-out force required to remove the devices from the LAA, a custom testing setup which could be attached to a Zwick Roell z010 tensile tester was designed and 3D-printed (Figure 3b). Elastomeric polyurethane (M1 Carbon, EPU) was used to fabricate an anatomically correct LAA and secured this to one end of a rigid adapter (Objet30 Scholar Stratasys, Veroblue) which connects to the load cell of the tensile tester. Six P-S occluders (with a Chicken Wing morphology that corresponded to the LAA in the testing rig) and six spherical occluders to six different volumes ($V_{inflation} \approx 50–200\%$) were then inflated. The occluders with an RTV-silicone prepolymer (Ecoflex 00–30, Smooth-on) blended with 10 wt % silicone thinner were backfilled (Smooth-on) which allowed for easier injection. After the

silicone was fully cured, a loop of Kevlar was threaded through the ostial surface of the occluder (Figure S6, Supporting Information). The occluder was properly positioned and oriented within the simulated LAA and secured the Kevlar string to the moving head of the tensile tester. Next, the occluder was pulled back out of the LAA at a rate of 25 mm min^{-1} while recording the tensile force ($n = 5$). The maximum tensile force applied to the occluder during this pull-out test was reported.

Embolism Tests

A custom benchtop flow-loop determined if the P-S or spherical occluders would embolize during the first 48 h of implantation (Figure 3c, and Figure S8, Supporting Information). This setup was modified from one described in a previous publication.[15] Briefly, a sealed, 3D-printed idealized left atrium was attached to two pumps (ZKWP03A, FORTRIC), a patient-specific silicone LAA, and a pressure transducer (0–15 PSI, TDH30-CG-0015–03-D004, Transducers direct; Figure S8, Supporting Information). A relay switch alternatively operates these pumps at physiological rates ($f \approx 1$ Hz). An external reservoir feeds and collects water from these pumps. By placing this reservoir at a height ≈15 in. below the flow loop, a pressure of $\Delta P \approx 15$ kPa was produced inside of the chamber. The occluder was then implanted into the simulated LAA and took pressure readings at 0, 24, and 48 h to ensure the desired physiological pressure range is maintained.

Occlusion Tests

A P-S occluder was attached to a programmable syringe pump (NE-1000, New Era Pump Systems Inc.) via plastic tubing before being correctly oriented inside of a 3D-printed, anatomically correct LAA (M1 Carbon, EPU; Figure S7, Supporting Information). An additional syringe and three-way valve were used to remove the air inside of the occluder. Water was then infused into the empty occluder using the syringe pump at a rate of 1 mL min^{-1}. A custom LabVIEW code was used to control and record the input volume. While the occluder was being inflated, water was continuously poured into the LAA. A small hole in the distal tip of the LAA allowed the water to flow around the occluder and out of the LAA in a steady stream. As the occluder inflated and conformed to the walls of the LAA, the volume of water flowing out of the LAA decreased. When water ceased flowing out of the LAA, the occluder was determined to have fully occluded the vessel, and the volume of infused liquid was recorded (n = 10). This volume was then compared to the known internal volume of the P-S occluders to determine the occlusion volume.

Computational Flow Dynamics

The geometry of the left atrium (with extension of ≈20 mm downstream of the mitral annulus) was reconstructed from segmentations of CT cardiac images. The spherical and P-S occluders were positioned inside the LAA. The fluid domain was then defined as the remaining volume inside of the atrium in either the spherical or P-S occluder models. Mass blood flows of the pulmonary veins as measured previously[41] were prescribed as the inlet boundary conditions. The flow profile was defined parallel to the pulmonary veins walls to minimize the influence of inlet curvature on inflow streamline. The cross section of the ventricle (outflow) was defined as an opening at zero-gauge pressure. The fluid domains of spherical and P-S occluders were discretized by 408 667 and 472 741 tetrahedral elements,

respectively (Figure 4). Increasing the number of the mesh elements by 25% resulted in a less than 5% variation in maximum wall shear stress on the occluders' walls, proving mesh independence. The blood flow was simulated in Ansys Fluent (Version 18.0) using a shear stress transport k-w model for a diastolic phase of 650 ms. Blood was modeled as Newtonian fluid with a density of 1050 kg m^{-3} and a dynamic viscosity of 3.5×10^{-3} kg m^{-1} s^{-1}. The atrium and vascular walls were assumed rigid, and no-slip boundary conditions were applied at the walls. The mitral valve was not included in either case to simplify the model.

Fourier-Transform Infrared Spectroscopy Tests

FTIR was performed using a Bruker Vertex V80V Vacuum FTIR system. EPU cubes ($V = 1$ cm^3) were printed and postprocessed to varying degrees. Samples were either cleaned of excess resin by wiping them with a Kimwipe, cleaned and washed in an isopropyl alcohol bath, or fully postprocessed (cleaned with Kimwipe, washed in isopropyl alcohol, UV cured, and thermally cured at 120 °C for 8 h). These samples were then swelled in THF solvent for 48 h to remove unreacted compounds from the printed EPU cube. FTIR was performed on the resulting solvent samples in attenuated total reflection mode in air. Spectra for the THF solvent and a control containing the photoinitiator (diphenyl(2,4,6-trimethylbenzoyl)phosphine oxide, Sigma Aldrich) were also measured to serve as comparisons.

Statistical Analyses

Sample size, mean, and standard deviation are reported for all data sets. No statistical methods were used to predetermine the sample sizes for the characterization of the performance of the occluders. All statistical analyses were performed in Origin (Academic Version, 2016) and Microsoft Excel (Excel for Mac, Version 15.32, 2017).

Code Availability

The LabVIEW and Arduino Uno codes that were used in this study can be made available upon request to the corresponding author.

Data Availability

The authors declare that all data supporting the findings of this study are available within the manuscript and the Supporting Information.

Image Acquisition

All photographs were taken with a Canon (EOS Rebel T3i).

Image Processing

Except where explicitly stated (i.e., where it is stated that the contrast was changed), photographs were only cropped and positioned in figures using Adobe Illustrator (CS6, Version 16.0.3), Adobe Photoshop (CS6, Version 12.0), and PowerPoint (Microsoft Office). SolidWorks (Education Edition, 2016) renderings were performed using PhotoView 360 Add-In feature. Geomagic Wrap (Version 2015) renderings were taken using the Snapshot

feature. Schematics were created using Adobe Illustrator. All arrows, dotted lines, and text were added to images in Adobe Photoshop or PowerPoint. All plots were created in Origin (Academic Version, 2016).

Supplementary Material

Refer to Web version on PubMed Central for supplementary material.

Acknowledgements

S.S.R. and C.A.A. contributed equally to this work. This work made use of the Cornell Center for Materials Research Facilities supported by the National Science Foundation under Award No. DMR-1120296. This work was supported by Weill Cornell Medical College Clinical & Translational Science Center (Grant No. TL1-TR-002386), the Army Research Office (Grant No. W911F-16-1-0095), and the Office of Naval Research (Grant No. N00014-17-1-2837).

References

[1]. Zhao H, Li Y, Elsamadisi A, Shepherd R, EML 2015, 3, 89.

[2]. Wallin TJ, Pikul JH, Bodkhe S, Peele BN, Mac Murray BC, Therriault D, McEnerney BW, Dillon RP, Giannelis EP, Shepherd RF, J. Mater. Chem. B 2017, 5, 6249.

[3]. Robinson SS, O'Brien KW, Zhao H, Peele BN, Larson CM, Mac Murray BC, van Meerbeek IM, Dunham SN, Shepherd RF, EML 2015, 5, 47.

[4]. Mac Murray BC, An X, Robinson SS, van Meerbeek IM, O'Brien KW, Zhao H, Shepherd RF, Adv. Mater 2015, 27, 6334. [PubMed: 26384472]

[5]. Morrison RJ, Hollister SJ, Niedner MF, Mahani MG, Park AH, Mehta DK, Ohye RG, Green GE, Sci. Transl. Med 2015, 7, 285ra64.

[6]. Lantada AD, Del Valle-Fernandez R, Morgado PL, Munoz-Garcia J, Sans JLM, Munoz-Guijosa JM, Otero JE, Ann. Biomed. Eng 2009, 38, 280. [PubMed: 19826955]

[7]. Sündermann SH, Gessat M, Cesarovic N, Frauenfelder T, Biaggi P, Bettex D, Falk V, Jacobs S, Interact. Cardio- Vasc. Thorac. Surg 2013, 16, 417.

[8]. D'Urso PS, Effeney DJ, Earwaker WJ, Barker TM, Redmond MJ, Thompson RG, Tomlinson FH, Br. J. Plast. Surg 2000, 53, 200. [PubMed: 10738323]

[9]. Brie J, Chartier T, Chaput C, Delage C, Pradeau B, Caire F, Boncoeur M-P, Moreau J-J, J. Craniomaxillofac. Surg 2013, 41, 403. [PubMed: 23218977]

[10]. Xu N, Wei F, Liu X, Jiang L, Cai H, Li Z, Yu M, Wu F, Liu Z, Spine 2016, 41, E50. [PubMed: 26335676]

[11]. Schwarzkopf R, Brodsky M, Garcia GA, Gomoll AH, Orthop. J. Sports Med 2015, 3, 232596711559037.

[12]. Mao Y, Xu C, Xu J, Li H, Liu F, Yu D, Zhu Z, Int. Orthop 2015, 39, 2023. [PubMed: 26285669]

[13]. Akhtar R, Sherratt MJ, Cruickshank JK, Derby B, Mater. Today 2011, 14, 96.

[14]. Su P, McCarthy KP, Ho SY, Heart 2008, 94, 1166. [PubMed: 17488765]

[15]. Robinson SS, Alaie S, Sidoti H, Auge J, Baskaran L, Avilés-Fernandez K, Hollenberg SD, Shepherd RF, Min JK, Dunham SN, Mosadegh B, Nat. Biomed. Eng 2018, 2, 8. [PubMed: 31015654]

[16]. Wolf PA, Abbott RD, Kannel WB, Stroke 1991, 22, 983. [PubMed: 1866765]

[17]. Blackshear JL, Odell JA, Ann. Thorac. Surg 1996, 61, 755. [PubMed: 8572814]

[18]. Landefeld SC, Beyth RJ, Am. J. Med 1993, 95, 315. [PubMed: 8368229]

[19]. Yu C-M, Khattab AA, Bertog SC, Lee APW, Kwong JSW, Sievert H, Meier B, Nat. Rev. Cardiol 2013, 10, 707. [PubMed: 24145892]

[20]. Moss JD, Curr. Cardiol. Rep 2014, 16, 448. [PubMed: 24408675]

[21]. Kong B, Liu Y, Huang H, Jiang H, Huang C,J. Thorac. Dis 2015, 7, 199. [PubMed: 25713737]

[22]. Lee C-H, Kim JB, Jung S-H, Choo SJ, Chung CH, Lee JW, Ann. Thorac. Surg 2014, 97, 124. [PubMed: 24075500]

[23]. Katz ES, Tsiamtsiouris T, Applebaum RM, Schwartzbard A, Tunick PA, Kronzon I, JACC 2000, 36, 468. [PubMed: 10933359]

[24]. Kanderian AS, Gillinov AM, Pettersson GB, Blackstone E, Klein AL, JACC 2008, 52, 924. [PubMed: 18772063]

[25]. O'Brien J, Al-hassan D, Ng J, Joshi M, Hague C, Chakrabarti S, Leipsic J, Int. J. Cardiovasc. Imaging 2014, 30, 819. [PubMed: 24599646]

[26]. Viles-Gonzalez JF, Kar S, Douglas P, Dukkipati S, Feldman T, Horton R, Holmes D, Y Reddy V, JACC 2012, 59, 923. [PubMed: 22381428]

[27]. Kolesky DB, Homan KA, Skylar-Scott MA, Lewis JA, Proc. Natl. Acad. Sci. USA 2016, 113, 3179. [PubMed: 26951646]

[28]. Mosadegh B, Xiong G, Dunham S, Min JK, Biomed. Mater 2015, 10, 034002. [PubMed: 25775166]

[29]. Anwar S, Singh GK, Varughese J, Nguyen H, Billadello JJ, Sheybani EF, Woodard PK, Manning P, Eghtesady P,JACC: Cardiovasc. Imaging 2017, 10, 953. [PubMed: 27450874]

[30]. Odent J, Wallin TJ, Pan W, Kruemplestaedter K, Shepherd RF, Giannelis EP, Adv Funct. Mater 2017, 27, 1701807.

[31]. Patel DK, Sakhaei AH, Layani M, Zhang B, Ge Q, Magdassi S, Adv. Mater. 2017, 29, 1606000.

[32]. Melchels FPW, Feijen J, Grijpma DW, Biomaterials 2010, 31, 6121. [PubMed: 20478613]

[33]. Bhattacharjee N, Parra-Cabrera C, Kim YT, Kuo AP, Folch A, Adv. Mater 2018, 30, 1800001.

[34]. Oskui SM, Diamante G, Liao C, Shi W, Gan J, Schlenk D, Grover W, Environ. Sci. Technol. Lett 2015, 3, 1.

[35]. Carroll RG, Elsevier's Integrated Physiology, Elsevier, Amsterdam 2007, pp. 91–98.

[36]. Akinapelli A, Bansal O, Chen JP, Pflugfelder A, Gordon N, Stein K, Huibregtse B, Hou D, Curr. Cardiol. Rev 2015, 11, 334. [PubMed: 26242188]

[37]. Koskinas KC, Chatzizisis YS, Antoniadis AP, Giannoglou GD, JACC 2012, 59, 1337. [PubMed: 22480478]

[38]. Vukicevic M, Mosadegh B, Min JK, Little SH, JACC: Cadiovasc. Imaging 2017, 10, 171.

[39]. Giannopoulos AA, Chepelev L, Sheikh A, Wang A, Dang W, Akyuz E, Hong C, Wake N, Pietila T, Dydynski PB, Mitsouras D, Rybicki FJ, 3D Print. Med 2015, 1, 3. [PubMed: 30050972]

[40]. Giannopoulos AA, Mitsouras D, Yoo S-J, Liu PP, Chatzizisis YS, Rybicki FJ, Nat. Rev. Cardiol 2016, 13, 701. [PubMed: 27786234]

[41]. Tu J, Inthavong K, Wong KKL, Computational Hemodynamics: Theory, Modelling and Applications, Springer, Berlin 2015.

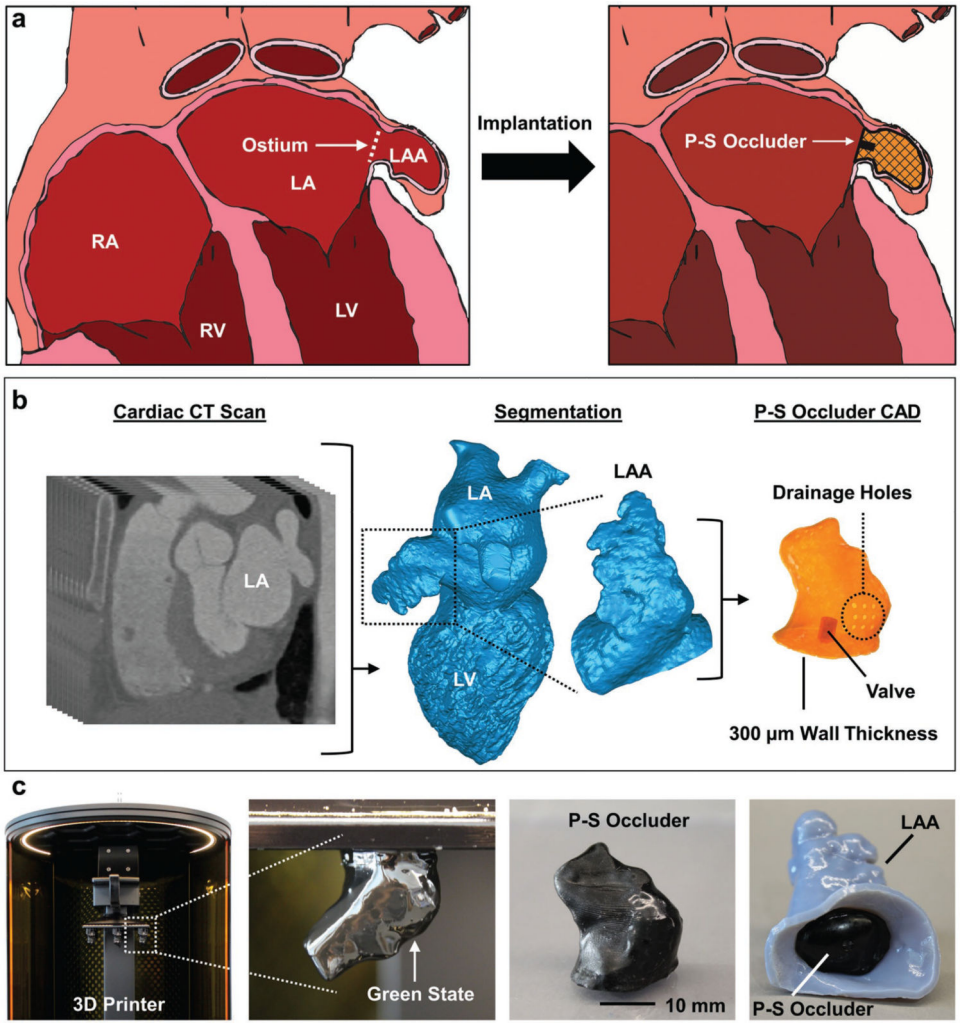

Figure 1.

Direct 3D printing of patient-specific (PS) left atrial appendage (LAA) occluder. a) Schematic of heart with right atrium (RA), right ventricle (RV), left atrium (LA), and left ventricle (LV) labeled. The ostium is the opening between the LA and LAA. A P-S occluder is implanted into the LAA and conforms to the surrounding tissue. b) CT segmentation of left heart blood volume, isolation of LAA, CAD design of P-S hollow occluder with 300 μm wall thickness, 3 mm diameter valve, and drainage holes for venting during printing. c) 3D printing of P-S occluder. The freshly printed part as a delicate *green body.* Final printed P-S occluder after cleaning and full cure. P-S occluder implanted into 3D-printed LAA.

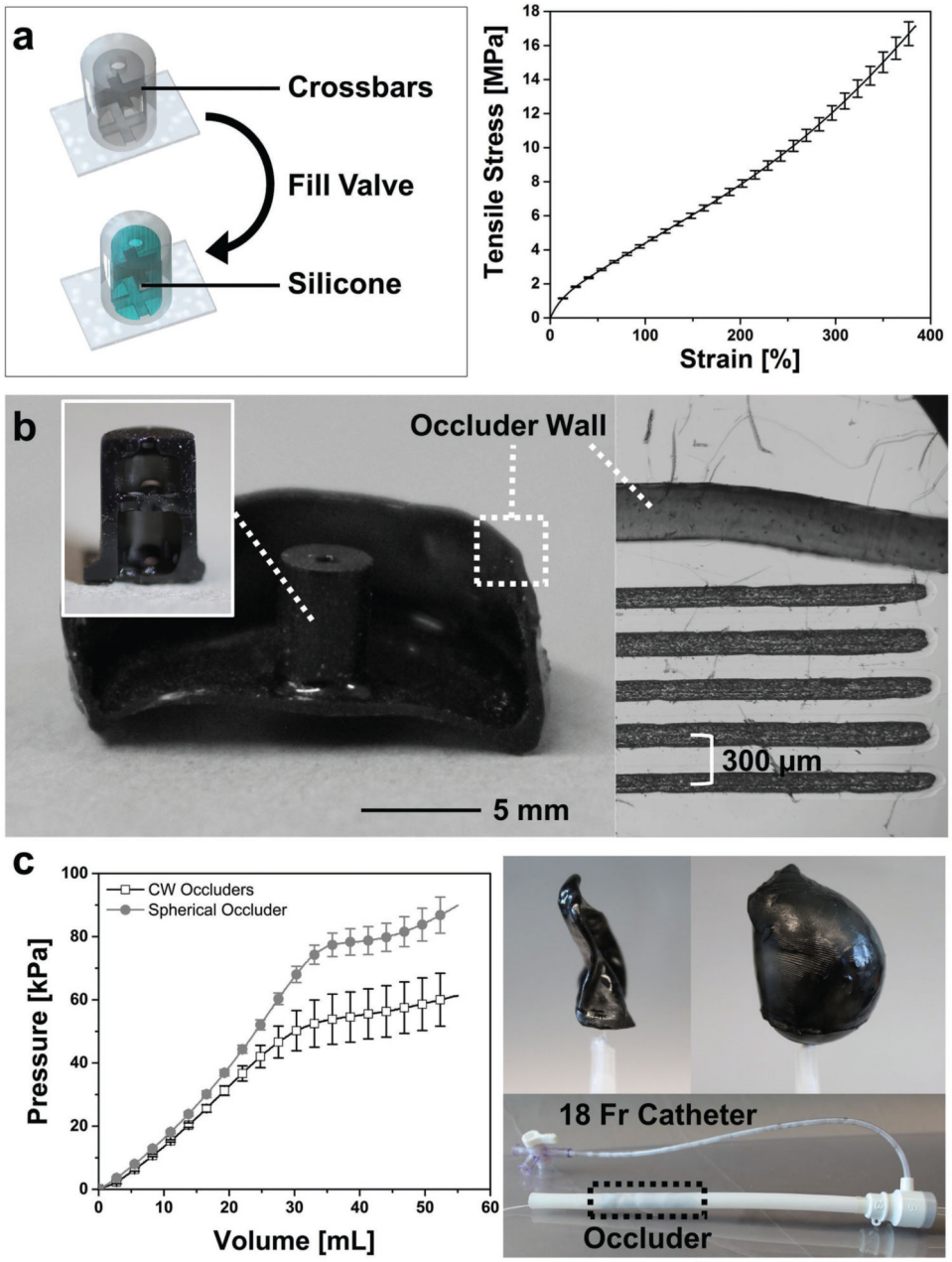

Figure 2.

Features of 3D-printed, patient-specific occluders. a) Schematic of printed valve before and after filling with silicone. The printed crossbars (black) lock the added silicone (blue) in position so no covalent bonding is necessary (left). The uniaxial tensile behavior of elastomeric polyurethane (EPU; $n = 11$, mean ± s.d.). b) Cross section of occluder with cross section of valve inset. Right: optical microscope image of cross section of occluder wall next to reticle for measuring wall thickness, $t \approx 318.6 \pm 49$ μm ($n = 9$, mean ± s.d. from 3 occluders). c) Comparison of P-S and spherical occluders pressure-volume behavior (left, $n = 7$, mean ± s.d.). Right top: image of P-S occluder evacuated and inflated to very large

volumes using air ($\Delta P > 50$ kPa) Right bottom, potential delivery method, P-S occluder within an 18 Fr catheter (outlined by dotted line).

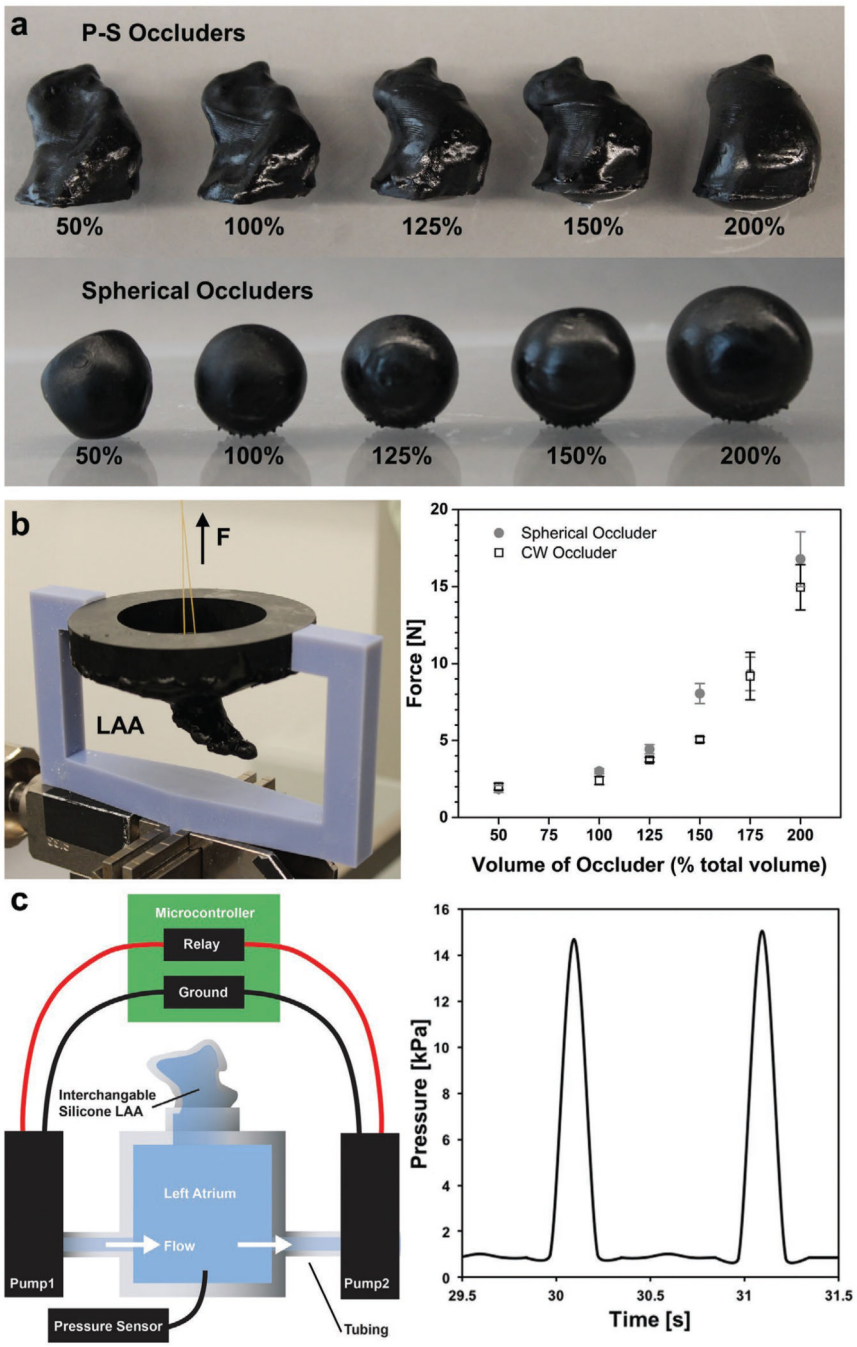

Figure 3.

Pull-out and embolism performance of patient-specific (PS) versus spherical occluders. a) P-S and spherical occluders filled with Ecoflex 00–30 up to $V_{\text{inflation}} \approx 200\%$. b) 3D-printed pull-out test jig attached to Zwick tensile tester (left). Force needed to pull occluder out of LAA when inflated by increasing amounts ($n = 5$, mean ± s.d.). c) Schematic of embolism test setup. P-S or spherical occluder was implanted into the silicone LAA for 48 h to see if occluder would embolize (left). Physiological pressure drops ($\Delta P_{\text{left heart}} \approx 15$ kPa) and frequencies ($f \approx 1$ Hz) were maintained throughout the 48 h.

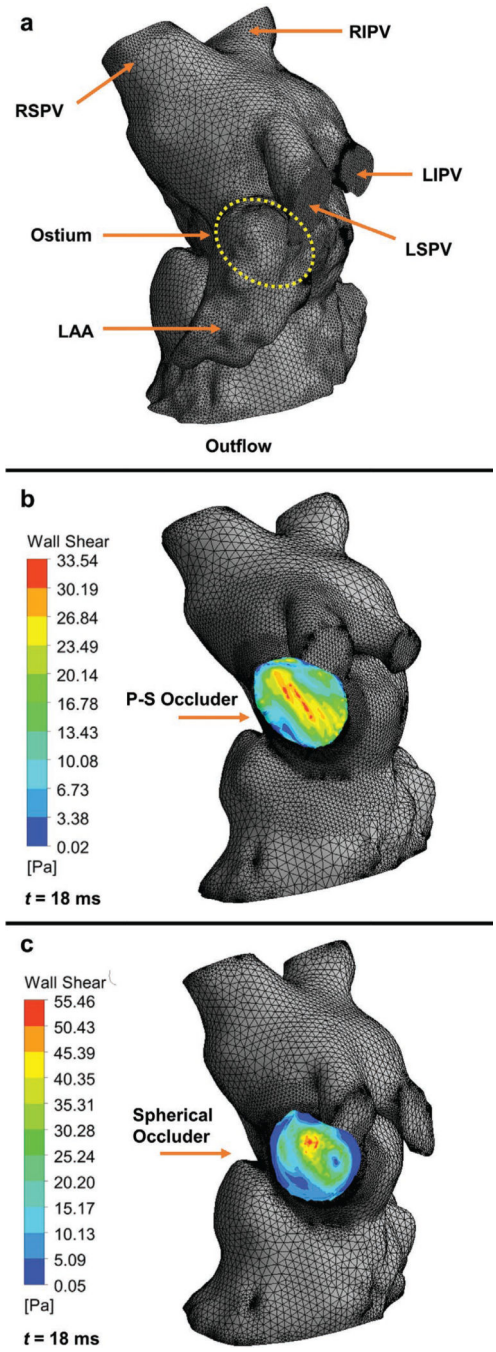

Figure 4.

Computational hemodynamics of the atrium facing wall of a patient-specific (PS) or spherical occluder. a) Fluid domains discretization with 441162 tetrahedron elements. Right superior pulmonary vein (RSPV), right inferior pulmonary vein (RIPV), left superior pulmonary vein (LSPV), and left inferior pulmonary vein (LIPV) are the inflow regions. The ostium is not visible from this surface view, but its position on the interior surface has been outlined using a yellow dotted line. The Chicken Wing morphology LAA has also been highlighted. The outflow region is the left ventricle, it has been cropped out. b) Model of left

heart with PS occluder within the LAA, it has 472 741 tetrahedron elements. The wall shear stress contour of the atrial wall of the occluder has been overlaid on the model. c) Model of left heart with spherical occluder within the LAA, it has 408 667 tetrahedron elements. The wall shear stress contour of the atrial wall of the occluder has been overlaid on the model. Note the areas of dark blue on the outer edges. These are located where crevices have formed between the occluder and the atrial wall.

Table 1.

Embolism and pull-out test results for occluders of various inflation volumes (n= 5, mean ± s.d.).

***V*inflation**	**50%**	**100%**	**125%**	**150%**	**200%**
Embolism test results					
P-S	Embolized	Stable	Stable	Stable	Stable
Spherical	Embolized	Stable	Stable	Stable	Tore LAA
Pull-out test results [N]					
P-S	2.0 ± 0.22	2.4 ± 0.27	3.8 ± 0.14	5.0 ± 0.19	14.9 ± 1.47
Spherical	1.9 ± 0.22	3.0 ± 0.17	4.4 ± 0.30	8.0 ± 0.64	16.8 ± 1.78